Laser Driven Ablative Surface Instability in IFE

By N. RUDRAIAH, TARA DESAI AND PREMA SRIDHARAN

National Research Institute for Applied Mathematics (NRIAM)
No.492/G, 7th Cross, 7th Block (West), Jayanagar, Bangalore – 560 082

and

UGC-DSA Centre in Fluid Mechanics, Department of Mathematics
Bangalore University, Bangalore – 560 001

Electricity is the most preferred form of energy as it can be easily produced, transported and converted into heat, light and motion. Eighty four percent of the world's electrical energy comes from fossil fuels such as coal, oil or gas. All of which are nonrenewable and the remaining sixteen percent of the world's electricity is supplied from 439 nuclear reactors in operation. In some countries a significant part of electricity comes from nuclear sources. Different types of reactors are operating in these countries and each country makes its own selection based on their suitability with respect to local conditions, availability of technology, availability of fuel, safety, manufacturing infrastructure, economy etc. The choice of reactors for Indian Nuclear Programme is also based on specific Indian conditions particularly available nuclear fuel resources. Due to fast depletion of fossil fuels and vagaries of mansoon, renewable energy sources are also important contributions, particularly for rural areas in India. However, bulk energy needs of industries and dense urban population requires large central generating stations to provide uninterrupted supply of electricity. One of the future effective centrally generating energies is the fusion energy.

In this regard the IAEA has identified Inertial Fusion Energy (IFE) and Magnetic Fusion Energy (MFE) as an alternate sources of energy. In addition, the Thermonuclear Reactor Energy (TNRE) is also going to be useful source of energy. The IAEA has identified the following major components of IFE Power Plants (i) Driver (ii) Fuel Pellet (iii) Chamber and (iv) Power Conversion. Recently significant advances in high energy drivers, such as high energy and high intensity lasers, pulsed power and intense ion beams and target physics experiments have led to a great expansion of the knowledge of inertial fusion science and its application. It has become possible to foresee the path towards IFE as a future energy source because of the progress observed in the high repetition rate reactor driver development. Laser compressed core densities in excess of 1000 tones solid densities have been demonstrated. In several countries (for example USA, Europe, Japan and so on), research projects have started to establish the scientific principle of ignition and high energy gain. In some countries mentioned above PW laser systems have been constructed to study the heating of compressed cores which are based on the new concept "fast ignition". These scientific studies will give important physics database to engineering in order to realize IFE as a commercial energy source.

This in view, IAEA has entrusted the following research objectives to CRP: (i) Technology assessment (ii) Interface issues, and (iii) system integration and assessment. We at the NRIAM proposed to study laser driven ablative surface instability. In ICF, it is shown that continuous inward acceleration of spherical shells by ablation pressure alters the outer surface. Here spherically symmetric calculations of the behavior of laser driven fusion targets have demonstrated major advantages of employing ablatively imploded spherical shells for obtaining optimum performance. The use of solid pellets in the form of shells opposed to solid sphere has been shown to reduce significantly the peak laser power required to drive successfully a target of fixed mass. To overcome the major inconvenience due to the location of segregation of inner skin of shells, hollow shells have been employed

(see Bocquet et al , 1990). However, the hollow shell targets are shown to be hydrodynamically unstable in the ablation region where the pressure and density are of opposite signs (Mccrory et al, 1976). The surface instability in this region is due to heavy fluid supported by a lighter fluid i.e. lighter fluid accelerating the denser fluid is similar to classical Rayleigh – Taylor (RT) instability but complicated by finite density scale lengths. The instability in the hollow shell may reduce the efficiency of the fusion reaction and there should be a mechanism to control this instability. In the present work we propose the use of porous shells instead of hollow shells for the resistance offered by the solid particles in a porous medium reduces the instability considerably. We show that the permeability of the porous region scaled with Reynolds number decreases considerable the growth rate of instability compared to that of a hollow shell resulting in increase of efficiency of the fusion reaction. To achieve this object we discuss the mathematical formulation in section 2. To derive the dispersion relation we use moment formulation in section 3 rather than the usual energy formulation. The actual difficulty that the discontinuity in classical shear that exists at the interface using the energy method is shown to over come using moment formulation. The dispersion relation is obtained in section 4. Several particular cases are derived in section 5 and the results are discussed in the final section.

2. Mathematical Formulation

The physical configuration to be studied consists of three-dimensional rectangular densely packed fluid saturated porous medium as shown in the fig.1. The basic equations for an incompressible heterogeneous fluid in the absence of inertia (because the porous layer is densely packed) is given by

$$\rho\frac{\partial \vec{q}}{\partial t} = -\nabla p - \frac{\mu}{k}\vec{q} - \rho g + \sum T_s \nabla_1^2 z_1\, \delta(z - z_s) \tag{2.1}$$

$$\nabla.\vec{q} = 0 \tag{2.2}$$

$$\frac{\partial \rho}{\partial t} + (\vec{q}.\nabla)\rho = 0 \tag{2.3}$$

where $\vec{q} = (u, v, w)$ are the components of Darcy velocity, μ the viscosity of the fluid, g the acceleration due to gravity, T the surface tension and z_s is the interface. Here, equation (2.1) is the Darcy equation in the presence of gravitational and surface tension forces and equation (2.3) is the condition for heterogeneity. Here, we are interested in studying the instability of the interface subject to linear theory using normal mode analysis in which all the dependent variables are assumed to be of the form

$$F(z) = f(z)\, E^{i(l\,x + m\,y) + n\,t} \tag{2.4}$$

where *l* and m are the horizontal wave numbers with $\alpha = \sqrt{l^2 + m^2}$ is the wave number and n is the frequency of oscillations.

Eliminating the pressure p from equation (2.1) using (2.2), (2.3) and (2.4), we get the stability equation

$$D(\rho Dw) + \frac{\mu}{n\,k} D^2 w - \alpha^2\left(n\,\rho + \frac{\mu}{k}\right)w + \frac{\alpha^2}{n^2} g\,(D\,\rho)w - \frac{\alpha^4}{n^2}\sum T_s \delta(z - z_s)w = 0 \tag{2.5}$$

3. Moment Formulation

We note that the analytical solution of (2.5) is difficult because of variation in density. In such cases, early work on RTI (see Chandrasekar, 1961) was based on energy approach, which requires boundary conditions on higher order derivatives of w. Recently, Mikaelean (1992) has discussed a simple model for ablative stabilization in the absence of a porous medium using the moment approach which does not require higher order boundary conditions. In this work, following Mikaelean (1986), we study RTI in a porous medium using the moment approach as explained below.

Multiplying equation (2.5) by w^m, and integrating with respect to z, we get

$$\frac{\alpha^2 g}{n^2} I_0 - \frac{\mu}{nk} I_1 = I_2 \tag{3.1}$$

where

$$I_0 = \int w^{m+1} D\rho \, dz - \frac{\alpha^2}{g} \sum T_s w^{m+1} \quad I_1 = \alpha^2 \sum w^{m+1} dz + m \int w^{m-1} (D w)^2 \, dz$$

$$I_2 = \alpha^2 \int \rho \, w^{m+1} \, dz + m \int \rho \, w^{m-1} (Dw)^2 \, dz$$

Here m = 1 gives energy formulation and m = 0 gives moment formulation.

4. Dispersion Relation

To derive the dispersion relation analytically, we assume the effect of density variation shown in fig and given by the following equation

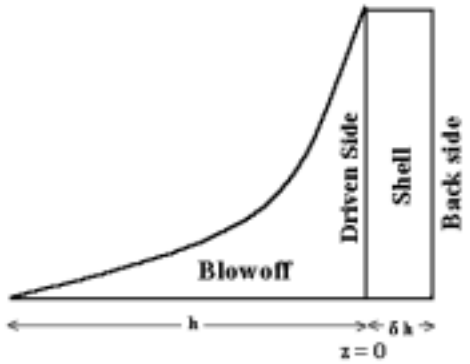

$$\rho(z) = \begin{cases} 0 & z \le -h \\ \rho_p e^{\beta z} & -h < z \le 0 \\ \rho_p & 0 \le z \le 0 \\ 0 & z > \delta h \end{cases} \tag{4.1}$$

FIG. 1 THE DENSITY PROFILE OF AN ABILATIVE DRIVEN TARGET

Here, the interface is the ablative surface, the region $-h \le z \le \delta h$ is called the blow off region and the region $0 \le z \le \delta h$ is called the shell, which is porous. The driven surface is at z=0 and the backside is at $z=\delta h$.
Using the classical solution (i.e. ρ is a constant) of (2.5), namely

$$w = e^{-\alpha |z|} \tag{4.2}$$

and the density given by (4.1) in (4.2) and taking m=0, we obtain

$$\frac{n^2}{g} + \frac{n}{g}\frac{\mu}{k} \frac{\int w \, dz}{\int \rho \, w \, dz} - \frac{\int w D\rho \, dz - \sum \frac{\alpha^2}{g} T_s w_s}{\int \rho \, w \, dz} = 0 \tag{4.3}$$

Using (4.2), we get

$$w=\begin{cases} e^{\alpha z} & \text{- h } \le z \le 0 \\ e^{-\alpha z} & 0 < z \le \delta h \end{cases}$$

Then,

$$\int w dz = \int_{-h}^{0} e^{\alpha z} dz + \int_{0}^{\delta h} e^{-\alpha z} dz = \frac{1}{\alpha}\left(2 - e^{-\alpha h} - e^{-\alpha \delta h}\right) \tag{4.4}$$

$$\int \rho w dz = \int_{-h}^{0} \rho_p e^{(\beta+\alpha)z} dz + \int_{0}^{\delta h} \rho_p e^{-\alpha z\, dz} = \frac{\rho_p}{\alpha+\beta}\left(1 - e^{-(\alpha+\beta)h}\right) + \frac{\rho_p}{\alpha}\left(1 - e^{-\alpha \delta h}\right) \tag{4.5}$$

Similarly, we get

$$\int D\rho w dz = \frac{\rho_p}{\alpha+\beta}\left((\alpha+\beta)\left(1 - e^{-\alpha \delta h}\right) - \alpha\left(1 - e^{-(\alpha+\beta)h}\right)\right) \tag{4.6}$$

Then, equation (4.3) using (4.4), (4.5) and (4.6) take the form

$$\frac{n^2}{g} + \frac{n}{g}\frac{\upsilon}{k}\frac{I_1}{I_2} - \frac{I_3}{I_2} = 0 \tag{4.7}$$

where

$$I_1 = (\alpha+\beta)\left(2 - e^{-\alpha h} - e^{-\alpha \delta h}\right), \qquad I_2 = \alpha\left(1 - e^{-(\alpha+\beta)h}\right) + (\alpha+\beta)\left(1 - e^{-\alpha \delta_h}\right),$$

$$I_3 = \alpha\left((\alpha+\beta)\left(1 - e^{-\alpha \delta h}\right) - \alpha\left(1 - e^{-(\alpha+\beta)h}\right) - \alpha^2(\alpha+\beta)\frac{T_s}{\rho_p g}\right)$$

We note that typical values of h are very large, usually $h \ge 500\,\mu$m (see Mikaelean 1992) and hence we consider here the case h→∞.

As h→∞, equation (4.7) take the form

$$\frac{n^2}{g} + \frac{n}{g}\frac{\upsilon}{k}\frac{f_1}{f_2} - \frac{f_3}{f_2} = 0 \tag{4.8}$$

where

$$f_1 = (\alpha+\beta)\left(2 - e^{-\alpha \delta h}\right), \qquad f_2 = \alpha + (\alpha+\beta)\left(1 - e^{-\alpha \delta h}\right),$$

$$f_3 = \alpha\left(\beta - (\alpha+\beta)e^{-\alpha \delta h} - \alpha^2(\alpha+\beta)\frac{T_s}{\rho_p g}\right)$$

From this equation, we derive the following particular cases for the dispersion relation.

5. Particular Cases :

5.1. Long Wavelength Perturbation

In this case, we consider long wavelength perturbation i.e. $\alpha<<\beta$. Then equation (4.8) reduces to

$$\frac{n^2}{\alpha g}+\frac{n}{\alpha g}\frac{\upsilon}{k}\frac{\left(2-e^{-\alpha\delta h}\right)}{\left(1-e^{-\alpha\delta h}\right)}+\frac{\alpha^2 T_S}{\rho_p g\left(1-e^{-\alpha\delta h}\right)}=1 \tag{5.1}$$

In the absence of porous media i.e. as $k\to\infty$, we get

$$\frac{n^2}{\alpha g}+\frac{\alpha^2 T_S}{\rho_p g\left(1-e^{-\alpha\delta h}\right)}=1 \tag{5.2}$$

We note that in the absence of surface tension, that is when Ts=0, we get the classical result of Taylor (1950).

$$n^2=\alpha g \tag{5.3}$$

Physically, this assumption of $\alpha<<\beta$ implies that the density variation is negligible for long wavelength.

5.2. Large Shell Thickness (i.e. $\delta h\to\infty$)

In this case equation (4.8) takes the form

$$\frac{n^2}{\alpha g}+\frac{2n}{\alpha g}\frac{\upsilon}{k}\frac{\alpha+\beta}{2\alpha+\beta}-\frac{(\alpha+\beta)-\alpha-\alpha^2(\alpha+\beta)\frac{T_S}{\rho_p g}}{2\alpha+\beta}=0 \tag{5.4}$$

This corresponds to a layer of infinite extent (i.e. $h\to\infty$, $\delta h\to\infty$).
In the absence of porous media i.e. $k\to\infty$, equation (5.4) reduces to

$$\frac{n^2}{\alpha g}-\frac{\beta-\alpha^2(\alpha+\beta)\frac{T_S}{\rho_p g}}{2\alpha+\beta}=0 \tag{5.5}$$

This is valid for an incompressible homogeneous inviscid fluid in the absence of porous media. In the absence of surface tension, the above equation reduces to the result of Mikaelean (1986), namely

$$\frac{n^2}{\alpha g}=\frac{\beta}{2\alpha+\beta}\ . \tag{5.5}$$

5.3. Short Wave Length Perturbation

For short wave length perturbation, that is $\alpha>>\beta$, equation (4.8) can be written as

$$\frac{n^2}{\alpha g}+\frac{n}{\alpha g}\frac{\upsilon}{k}-\frac{\frac{\beta}{\alpha}-e^{-\alpha\delta h}-\frac{\alpha^2 T_S}{\rho_p g}}{2-e^{-\alpha\delta h}}=0 \tag{5.7}$$

As $\delta h\to\infty$, this equation takes the form

$$\frac{n^2}{\alpha g}+\frac{n}{\alpha g}\frac{\upsilon}{k}-\frac{1}{2}\left(\frac{\beta}{\alpha}-\frac{\alpha^2 T}{\rho_p g}\right)=0 \tag{5.8}$$

In the absence of porous media, the above equation reduces to

$$\frac{n^2}{\alpha g}-\frac{1}{2}\left(\frac{\beta}{\alpha}-\frac{\alpha^2 T_S}{\rho_p g}\right)=0 \tag{5.9}$$

In the absence of surface tension, this equation reduces to

$n^2 = 0.5\,\mathrm{g}\,\beta$

which is half the classical value of Rayleigh (1900) for the exponential density profile.

5.4. Absence of Shell Region

In the absence of shell region i.e. δh=0, the equation (4.8) becomes

$$\frac{n^2}{\alpha g}+\frac{n}{\alpha g}\frac{\upsilon}{k}\frac{(\alpha+\beta)}{\alpha}+\alpha(\alpha+\beta)\frac{T_s}{\rho_p g}+1=0 \tag{5.10}$$

In the absence of porous media, this reduces to

$$\frac{n^2}{\alpha g}+\alpha(\alpha+\beta)\frac{T_s}{\rho_p g}+1=0 \tag{5.11}$$

In the absence of surface tension, this equation reduces to

$n^2 = -\alpha g$

which is the classical result of Taylor (1950).

5.5. Finite Shell Thickness

In this case δh is finite. We note that equation (4.1) divides the density profile into two classes such as thick profile defined as $\beta\,\delta h \geq 1$ and a thin profile defined as $\beta\,\delta h<1$. Then, equation (4.8) takes the form

$$\frac{n^2}{\alpha g}+\frac{n}{\alpha g}\frac{\upsilon}{k}\frac{(\alpha+\beta)\left(2-e^{-\alpha\delta h}\right)}{\alpha+(\alpha+\beta)\left(1-e^{-\alpha\delta h}\right)}-\frac{\beta-(\alpha+\beta)e^{-\alpha\delta h}-\alpha^2(\alpha+\beta)\dfrac{T_S}{\rho_p g}}{\alpha+(\alpha+\beta)\left(1-e^{-\alpha\delta h}\right)}=0 \tag{5.12}$$

The reduction of the growth rate below the classical, namely, $n(\alpha g)^{-0.5}$ is plotted using the equation (5.12).

Let $n = n_1\sqrt{\alpha\,\mathrm{g}}$; $\quad \beta\,\delta\mathrm{h} = \mathrm{h}_1$; $\quad \alpha\,\delta\mathrm{h} = \alpha_1$;

then, equation (5.12) takes the form

$$n_1^2 + n_1 f_4 - f_5 = 0 \tag{5.13}$$

where

$$f_4 = \frac{(\alpha_1+h_1)\left(2-e^{-\alpha_1}\right)}{R\sqrt{\alpha_1}\left[\alpha_1+(\alpha_1+h_1)\left(1-e^{-\alpha_1}\right)\right]}, \quad f_5 = \frac{h_1-(\alpha_1+h_1)\left(e^{-\alpha_1}+\dfrac{\alpha_1^2}{B}\right)}{\alpha_1+(\alpha_1+h_1)\left(1-e^{-\alpha_1}\right)}$$

where R is the modified Reynolds number based on the classical frequency and B is the Bond number.

Equation (5.13) has two roots given by

$$n_1 = 0.5(-f_4 \pm \sqrt{f_4^2 + 4 f_5}) \qquad (5.14)$$

These are the required dispersion relations. We note that f_5 is always negative and hence n_1 and n_2 may be real or complex depending on $f_4^2 > f_5$ or $f_4^2 < f_5$ with a negative real part. The numerical computation shows that n_1 and n_2 are complex conjugates, and hence the system is oscillatory stable, i.e. over stable. Equation (5.14) is computed numerically for three thick profiles $\beta\delta h = 5, 10, 20$ and one thin profile βδh =0.5, where n $(\alpha g)^{-0.5}$ is drawn against $\beta\delta$h , and are depicted in figs. 2 (a) to 2 (e). The results are discussed in the next section.

6. Conclusions

The linear RTI of ablation surface is investigated by considering a three-dimensional densely packed porous shell of different thickness h_1 (=αδh, large, small and zero) and for large and small wavelength perturbations. The dispersion relation is computed numerically for different values of h_1, modified Reynolds number R = 10 and 100 and Bond number B = 0.1 to 0.4 and the results are shown in Figs. 2(a) to 2(e). We see from fig. 2(a) that for R= 10 and different h1 the system is always stable. However, for R = 100 and for small h1 the system is stable, whereas for increase in h1 all the three modes of instability exist and the system moves from unstable to stable state and approaches asymptotically to the neutral state (see fig (2b)). The dispersion relation is also computed for different values of modified Reynolds number for h_1=0.5 in fig (2c) and h_1= 5 in fig (2d). In both the cases we see that the increase in R decreases the growth rate and approaches towards more stable state. The increase in R means the decrease in growth rate and hence more suitable for control of stability which is favourable to increase the efficiency of IFE power plant.

The dispersion relation is also computed for different values of Bond number B and the results are depicted in fig 2(e). For all values of B upto 0.03 the system is stable. However, for B=0.01 the growth rate decreases for α_1 upto 0.5 and then approaches asymptotically the neutral curve. For other values of B the growth rate decreases for α = 0.6 and then approaches asymptotically neutral curve.

Acknowledgements

The authors gratefully acknowledge the financial support of IAEA for this work under its contract no.11534/R0/RBF.

References :

1. Bocquet, Blondeau, R, Poitrault, L, Badeau, J.B, Dumont, R, Power generation technology etd by Richard Knox,P. 141-146, 1990.
2. Chandrasekar, S, Hydrodynamic and hydromagnetic stability, oxford clarendon press, 1961.
3. Maccrory, R,L and Morse, R.L, Physics of Fluids,19, p 175, 1976.
4. Mikaelean, K,O, Phys Rev A, 33 (2), P 1216, 1986.
5. Mikaelean, K,O, Phys Rev A, 46 (10), P62, 1992.
6. Rayleigh, Scientific Papers II, Cambridge, England.
7. Taylor, G, I, Proc Roy Soc (Lond) A, 201, P6, 1950.

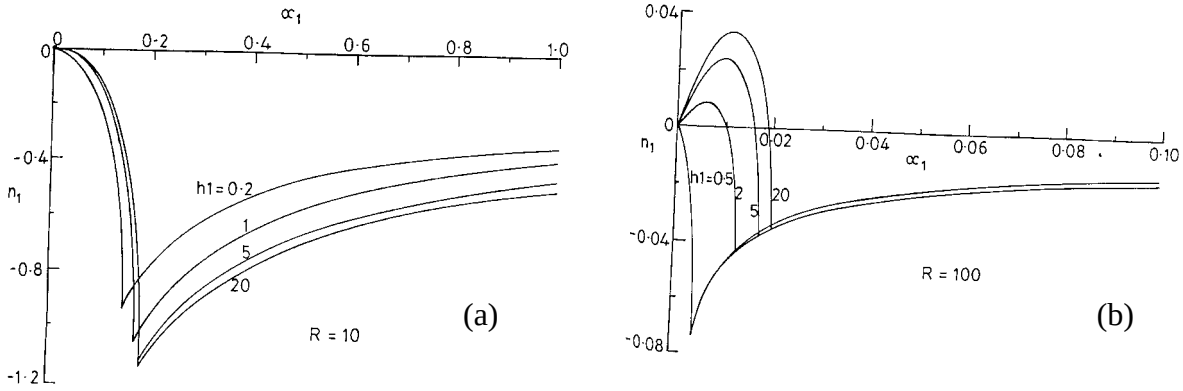

FIG. 2 a & b – Re (n_1) Vs. α_1 FOR DIFFERENT VALUES OF h_1

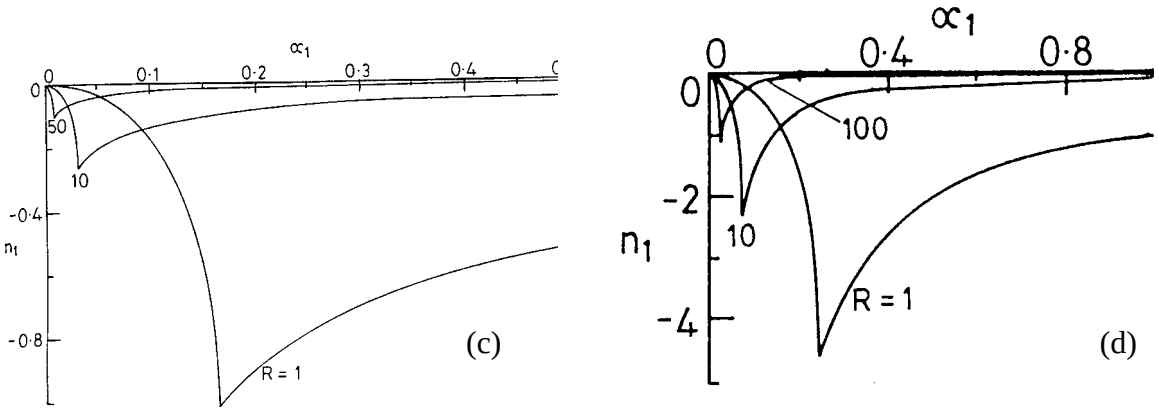

FIG. 2 c & d – Re (n_1) Vs. α_1 FOR DIFFERENT VALUES OF R

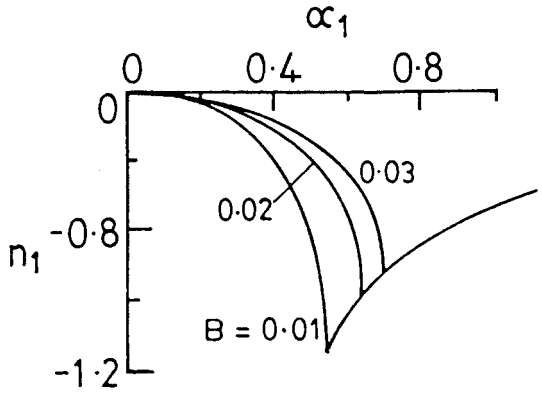

FIG. 2 e – Re (n_1) Vs. α_1 FOR DIFFERENT VALUES OF B

FIG. 2 c – Re (n_1) Vs. α_1 FOR DIFFERENT VALUES OF R

FIG. 2 d – Re (n_1) Vs. α_1 FOR DIFFERENT VALUES OF R

FIG. 2 e – Re (n_1) Vs. α_1 FOR DIFFERENT VALUES OF R